Journal Pre-proofs

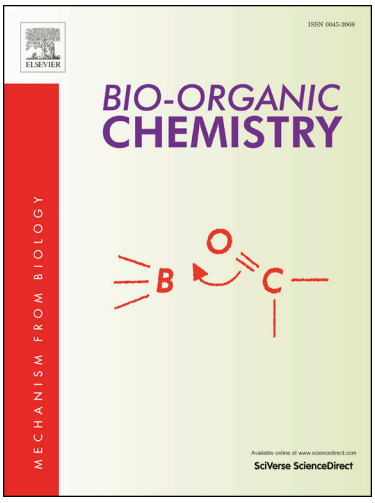

Synthesis and neuroprotective effects of novel chalcone-triazole hybrids

Pichjira Sooknual, Ratchanok Pingaew, Kamonrat Phopin, Waralee Ruankham, Supaluk Prachayasittikul, Somsak Ruchirawat, Virapong Prachayasittikul

PII: S0045-2068(20)31682-5
DOI: https://doi.org/10.1016/j.bioorg.2020.104384
Reference: YBIOO 104384

To appear in: *Bioorganic Chemistry*

Received Date: 27 June 2020
Revised Date: 16 September 2020
Accepted Date: 14 October 2020

Please cite this article as: P. Sooknual, R. Pingaew, K. Phopin, W. Ruankham, S. Prachayasittikul, S. Ruchirawat, V. Prachayasittikul, Synthesis and neuroprotective effects of novel chalcone-triazole hybrids, *Bioorganic Chemistry* (2020), doi: https://doi.org/10.1016/j.bioorg.2020.104384

Synthesis and neuroprotective effects of novel chalcone-triazole hybrids

Pichjira Sooknual[a], Ratchanok Pingaew[a,*], Kamonrat Phopin[b,c,*], Waralee Ruankham[b], Supaluk Prachayasittikul[d], Somsak Ruchirawat[e,f,g], Virapong Prachayasittikul[c]

[a]*Department of Chemistry, Faculty of Science, Srinakharinwirot University, Bangkok 10110, Thailand*

[b]*Center for Research and Innovation, Faculty of Medical Technology, Mahidol University, Bangkok 10700, Thailand*

[c]*Department of Clinical Microbiology and Applied Technology, Faculty of Medical Technology, Mahidol University, Bangkok 10700, Thailand*

[d]*Center of Data Mining and Biomedical Informatics, Faculty of Medical Technology, Mahidol University, Bangkok 10700, Thailand*

[e]*Chulabhorn Research Institute, Bangkok 10210, Thailand*

[f]*Program in Chemical Biology, Chulabhorn Graduate Institute, Bangkok 10210, Thailand*

[g]*Center of Excellence on Environmental Health and Toxicology (EHT), CHE, Ministry of Education, Thailand*

***** Corresponding authors

Tel: 662-649-5000 ext 18253

E-mail: ratchanok@g.swu.ac.th (R. Pingaew)

Tel: 662-441-4376

E-mail: kamonrat.php@mahidol.ac.th (K. Phopin)

Abstract

The development of novel neuroprotective agents is urgently needed for the treatment of neurodegenerative diseases, affecting aging individuals worldwide. In this study, a new series of chalcone-triazole hybrids (**6a-g**) were synthesized and evaluated for their biological properties including cytotoxicity, antioxidant, anti-apoptosis, and neuroprotection using SH-SY5Y cells. The results showed that **6a** and **6e** provided neuroprotection in oxidative stress-induced neuronal cell damage. Both compounds significantly improved the morphology of neurons and obviously increased cell survival rate of neuronal cells induced by oxidative stress. Additionally, **6a** and **6e** counteracted H_2O_2-induced mitochondrial dysfunction, which was supported by maintaining mitochondrial membrane potential, attenuating BAX protein, and increasing BCL-2 protein within the mitochondria as well as upregulating SOD2 mitochondrial antioxidant enzyme. Interestingly, these compounds promoted neuroprotection via SIRT-FOXO3a signaling pathway similar to resveratrol. The data indicated that the chalcone-triazole derivatives (**6a** and **6e)** could be considered to be promising compounds toward the discovery of disease-modifying candidates for a neurodegenerative therapy.
Keywords: Chalcone; Triazole; Antioxidant; Oxidative stress; Neurodegeneration

1. Introduction

Neurodegenerative disorders are characterized by memory loss, mental abilities, and physical changes in the brain. Recently, the most considered neurodegenerative diseases are Alzheimer's disease (AD)

and Parkinson's disease (PD). The incidence of patients with AD and PD have dramatically increased around the world particularly in aging population. The medicines are available, but with no effective treatment and side effects. Mostly, therapeutic medicines for neurodegenerative diseases were developed based on the existing drugs to relieve symptoms of neuronal damage (1). Addressing the global health concerns, new strategies that are able to counteract the substantial increase of cases are still needed (2, 3).

Many lines of evidence have indicated that neurodegeneration is prone to oxidative damage sharing common pathophysiologic mechanisms including mitochondrial dysfunction, protein aggregation, and neuroinflammation, leading to neuronal death (1, 3). Excessive production of reactive oxygen species (ROS) results in the damage of proteins, lipids, and DNA, causing oxidative stress (4).

One of the neuroprotective strategies for the treatment is to discover multipotential treatments i.e., antioxidant, anti-apoptotic, anti-inflammation, and target different mechanisms of neurodegeneration, which could stop the progression of diseases or delay the transition from the preclinical to the clinical stage (5). Therefore, the study has been directed to the discovery of promising natural and synthetic compounds for treatment of neurodegenerative diseases. Various natural and synthetic compounds i.e., chalcone and 1,2,3-triazole analogs have been reported to exert neuroprotective effects (6-9).

Chalcone (1,3-diaryl-2-propen-1-one, Fig. 1), the flavonoid family of natural product commonly found in vegetables, fruits, and spices, possesses a broad spectrum of biological activities including anticancer, anti-inflammatory, antioxidant, antimicrobial, antidiabetic, and anti-neurodegeneration (6, 7, 10-13). Chalcone based-compounds have been extensively studied with the aim to prevent the neurodegenerative disorders (12), and suggested to be used as a multi-functional candidate against multi-resistant AD in the future (12-29). Among them, naturally-occurring chalcones such as licochalcones (A and E) and xanthohumol (Fig. 1) could activate Nrf2, which is responsible for the oxidative properties (27-29).

1,2,3-Triazoles are nitrogen heterocycles existing in a diverse range of biologically active molecules due to their distinct properties. They are capable of forming hydrogen bonds

with many biomolecular targets, highly stable to metabolic degradation, and less undesired effects (8, 9, 30). The 1,2,3-triazole can be conjugated with various bioactive compounds such as quinolone (31), triazine (32), chromenone (33), lipoic acid (34), and tacrine (35) rendering them as multi-functional molecules for treatment of neurodegenerative disorders.

Various chalcone-triazole hybrids showing different biological activities have been reported. The linking of chalcone and 1,2,3-triazole units leads to the hybrids with better biological activities than their parent pharmacophoric units (36-41). Considering the pharmacophore of bioactive chalcones which bear 4-hydroxyphenyl keto group (Fig. 1), thus, novel series of chalcone-triazole hybrids were designed by replacing the 4-hydroxyl group with 1,2,3-triazole ring containing 4-substituents (scheme 1). The chalcone-triazole hybrids (**6a-g**) were synthesized and evaluated for their neurotoxicity, anti-apoptosis, antioxidant, and molecular mechanisms underlying neuroprotection, which could represent valid candidates for the development of new potential therapeutics.

2. Results and discussion

2.1 Chemistry

The chalcone-triazole hybrids **6a-g** were synthesized as illustrated in scheme 1 (42). Aminochalcone **3** was prepared by the base-catalyzed Claisen-Schmidt condensation of 3,4-dimethoxybenzaldehyde **1** and 4-aminoacetophenone **2** . Subsequently, diazotization reaction of the aminochalcone **3** using sodium nitrite and sodium azide in a mixture of glacial acetic acid and concentrated hydrochloric acid afforded azidochalcone **4**. In the final step, the copper(I)-catalyzed azide alkyne cycloaddition (CuAAC) of the azido compound **4** and alkynes **5** was performed to afford the novel hybrids **6a-g** in good yields (73-89%). The alkynes **5a-g** were derived from the alkylation of the corresponding phenol derivatives with propargyl bromide.

Structures of all chalcones (**6a-g**) were confirmed by ^{1}H NMR, ^{13}C NMR and HRMS data. The synthesized chalcones displayed molecular ion peaks corresponding to their molecular formulas. ^{1}H NMR spectra showed a methine proton of the triazole ring as the singlet at δ 9.0-9.2 ppm, and a methylene proton attached to triazole group displayed as the singlet at δ 5.2-5.5 ppm. The chalcone moiety showed two doublets of olefinic protons with the coupling constant (*J*) values of 15-16 Hz indicating that the *trans*-configuration was represented. In addition, ^{13}C NMR spectra showed carbonyl carbon at δ in the range of 188-

189 ppm. The newly synthesized hybrids (**6a-g**) contain various substituents (R) such as phenyl, substituted phenyl, and naphthalenyl groups.

2.2 Biological activities

2.2.1 Chalcone-triazole derivatives display no cytotoxicity in Vero cells

These compounds (**6a-g**) were evaluated for cytotoxicity using healthy cell line (Vero) derived from African green monkey kidney. The cytotoxicity (IC_{50}) values are shown in Table1. All chalcone-triazole derivatives were low cytotoxic toward the normal Vero cell line (IC_{50} > 50 µg/mL).

2.2.2 Chalcone-triazole derivatives improve cell viability of SH-SY5Y cells treated with H_2O_2

With all the target compounds in hands, their neuroprotective properties were assessed with the hope of preventing neuronal cell death. Firstly, the neurotoxicity of chalcone-triazole derivatives (**6a-g**) in neuroblastoma SH-SY5Y cells was evaluated. The neuronal cells were treated with various concentrations (0.1-100 µM) of the synthetic chalcone-triazole compounds, which needed to present toxicity less than 10% for maintaining the cell growth. Hydrogen peroxide (H_2O_2) can easily generate exogenous free radicals and highly react as ROS, which is a suitable model for studying an oxidative stress in neurodegenerative diseases. There is a wide variability of H_2O_2 concentration-induced toxicity ranging from 0.1 to 1 mM that has been observed in different primary cell cultures or cell lines. Specifically, neurons are particularly sensitive to H_2O_2-induced cytotoxicity (43, 44). In order to represent the oxidative stress model, 400 µM of H_2O_2 was added to SH-SY5Y cells for 24 h incubation, accompanied by compounds **6a** and **6e** pretreatment.

As shown in Table 1, treatment with 400 µM H_2O_2 significantly reduced cell viability (63.94 ± 2.06%), in comparison with H_2O_2 untreated cells, which indicated that H_2O_2 model was successfully employed. Among chalcone-triazole derivatives, the results showed that **6b**, **6c**, **6d**, **6f**, and **6g** at 1 µM could not significantly improve the survival rate of H_2O_2-treated neuronal cells. On the other hand, pretreatment with **6a** (87.82 ± 5.08%) and **6e** (87.16 ± 1.99%) reversed the reduction of cell viability compared with H_2O_2 treatment alone. Similar result was noted for resveratrol (86.08 ± 4.53%), which is a well-known antioxidant (Fig. 2a). Resveratrol (3,5,4-trihydroxy-*trans*-stibene, Fig. 1) is a natural polyphenolic compound mainly found in fruit and vegetables, especially grape seed. It can directly scavenge free radical and upregulate endogenous antioxidant enzymes, implying the protection of cell

viability indirectly. Many reports documented that resveratrol can cross blood-brain barrier and exerts neuroprotective properties in different *in vitro* and *in vivo* models of neurodegeneration (4, 44, 45). Moreover, the morphological changes of neurons were observed under a microscope. The cells were shrunk, detached, and become round shape in H_2O_2-treated cells in contrast to the pretreatment with **6a** and **6e** (Fig. 2b).

Amyloid cascade hypothesis is proposed for the main neuropathological hallmark of AD and dementia which is responsible for several molecular mechanisms leading to oxidative stress, synaptic plasticity, mitochondrial alteration, membrane permeability, and inflammation. Amyloid-β (Aβ) oligomer is widely regarded as the most harmful and major pathogenic form of amyloid plaques (46-48). In order to evaluate the ability of **6a** and **6e** against amyloid aggregation to prevent neurodegenerative diseases outstandingly AD patients, the cells were pretreated with **6a** and **6e** in the presence or absence of 10 μM $A\beta_{1\text{-}42}$ oligomer for 3 h. The $A\beta_{1\text{-}42}$ oligomer was performed according to a previous procedure (49). The confirming toxicity of the 10 μM $A\beta_{1\text{-}42}$ oligomer to neurons was investigated (80.73 ± 1.96%) as previously reviewed (47, 50). The results indicated that **6a** (96.32 ± 5.26%) and **6e** (98.02 ± 6.57%) prevent $A\beta_{1\text{-}42}$ oligomer-induced cytotoxicity similar to resveratrol (93.32 ± 3.35%) (Fig. 2c). Therefore, compounds **6a** and **6e** at 1 μM were selected for the subsequent experiments to determine neuroprotective effects against the oxidative damage.

*2.2.3 Pretreatment with **6a** and **6e** diminishes apoptotic profiles in H_2O_2-treated SH-SY5Y cells*

Both synthesized compounds (**6a** and **6e**) were evaluated as anti-apoptotic agents against H_2O_2-treated SH-SY5Y cells. Resveratrol was used as a reference compound. The results showed that H_2O_2-treated cells led to higher apoptosis (28.07 ± 2.03%) (Fig. 3a). Pretreatment with **6a** and **6e** did not affect the proportion of total apoptotic cells. Interestingly, **6a** and **6e** displayed anti-apoptotic property against oxidative damage showing apoptotic decline (20.93 ± 2.17% and 17.53 ± 2.57%) similar to the resveratrol (16.8 ± 1.02%) compared with the H_2O_2 group (Fig. 3a). It has been documented that BCL-2 family including anti-apoptotic BCL-2 and pro-apoptotic BAX proteins, which plays an important role in apoptotic system of the mitochondria, so the levels of BAX and BCL-2 proteins, were evaluated by Western blotting (Fig. 6a and 6b). Normally, the anti-apoptotic BCL-2 protein modulates the pro-apoptotic BAX activation at the mitochondria to inhibit cell damage.

Under the oxidative stress condition, the BCL-2 protein cannot modulate the activation of BAX leading to outer mitochondrial membrane disruption. Pro-apoptotic cytochrome c (Cytc) escapes from BAX oligomeric pores and promotes caspase cascade. An obvious apoptotic series of biochemical and morphological characteristics were occurred, comprising nuclear condensation, chromosomal DNA fragmentation, cytoplasmic membrane blebbing, phosphatidylserine flipping, and cell shrinkage (51, 52).

As expected, the level of BAX protein expression was significantly increased up to 121.9 ± 1.34% upon H_2O_2 induced oxidative stress, while the BCL-2 protein expression was significantly decreased (69.84 ± 4.55%) compared with the control. Surprisingly, the changes of BAX and BCL-2 protein expressions were restored by pretreatment with **6a** (BAX; 106.7 ± 3.93% and BCL-2; 91.56 ± 5.10%) and **6e** (BAX;110.4 ± 2.26% and BCL-2; 89.5 ± 6.03%) in comparison with the H_2O_2 group. The results suggested that derivatives **6a** and **6e** promote anti-apoptotic activities similar to the resveratrol (BAX; 99.43 ± 3.55% and BCL-2; 89.67 ± 2.62%) as outlined in Fig. 6a and 6b.

*2.2.4 Pretreatment with **6a** and **6e** potentiates* mitochondrial membrane potential

Mitochondrial membrane potential is one of the sensitive indicators of functional mitochondrial status, which is declined due to an excessive ROS accumulation. Several lines of research have reported that measurement of mitochondrial membrane potential prominently provides an early stage of apoptosis (51-54). To identify further biological properties of chalcone-triazole derivatives (**6a** and **6e**) in neuroprotection, mitochondrial membrane potential was investigated using SH-SY5Y cells treated with **6a** and **6e** under oxidative stress. Briefly, the cells were incubated in the medium containing 1 μM of **6a** and **6e** for 3 h prior to 400 μM H_2O_2 for a further 24 h. As shown in Fig. 4a, the cells treated with H_2O_2 significantly decreased the percentage of mitochondrial membrane potential (87.28 ± 0.83%), compared with the control. The levels of mitochondrial membrane potential were not affected by **6a** and **6e** treatments compared with the unexposed cells. However, for **6a** and **6e**-pretreated cells, the mitochondrial membrane potential induced by H_2O_2 was markedly increased to 108.1 ± 3.79% and 101.6 ± 4.45%, respectively in comparison with the H_2O_2 alone. The spectrometric results showed that the fluorescence intensity of H_2O_2 group was observed to be markedly lower than the control, however, it was attenuated by pretreatment with either **6a** or **6e** in the same manner as the resveratrol (Fig. 4b). The data indicated that **6a**

and **6e** are able to modulate the levels of mitochondrial membrane potential, which can clarify the molecular mechanism underlying the inhibitory effect of **6a** and **6e** against the apoptosis (Fig. 3a).

*2.2.5 Treatment of **6a** and **6e** attenuates the ROS levels in H_2O_2-induced SH-SY5Y cells*

ROS has been reported to be closely associated with the neurodegeneration. When free radical production and detoxification are unbalance, the over accumulation of ROS damages the neurons by attacking several biological components including nucleic acids, proteins, and lipids resulting in oxidative stress and cellular apoptosis. Antioxidants can be used as potential therapeutics to scavenge the ROS production (1, 4, 5). To determine the inhibition of ROS production associated with **6a** and **6e** in H_2O_2-induced oxidative damage in SH-SY5Y cells, the cellular DCFDA assay was performed. Previous publications focused on the possible role of H_2O_2, which can mediate ROS production in SH-SY5Y cells by disturbing oxidant and antioxidant defenses (55-58). We also provided that H_2O_2 evoked ROS-induced neurotoxicity in *in vitro* model. After the neurons were exposed to 400 μM of H_2O_2 for 24 h, ROS production was significantly increased (130.7 ± 3.93%) compared with the unexposed cells (Fig. 5a). The experiments also exhibited that pretreatment with **6a** and **6e** did not alter the intracellular ROS levels, on the other hand, pretreatment with **6a** and **6e** further declined the induction of ROS caused by H_2O_2 (110.4 ± 5.12% and 109.9 ± 6.88%, respectively) in comparison with the H_2O_2 exposure. Similarly, the fluorescence intensity was strongly reduced in the cells exposed to **6a** and **6e** compared with the H_2O_2 group (Fig. 5b).

A set of antioxidant enzymes, including glutathione (GSH), catalase (CAT), and superoxide dismutase (SOD), plays a predominant role in mitigating extensive oxidative damage, impairment of the cellular functions, and mitochondrial dysfunction. SOD is one of the first effective intracellular antioxidant defense against ROS. Especially, SOD2 is located inside the mitochondria which catalyzes the reaction of superoxide into the less reactive O_2 and H_2O_2 (54, 59, 60). Additionally, Western blot analysis further confirmed the reduction of SOD2 mitochondrial antioxidant enzyme in H_2O_2-treated cells (66.56 ± 2.96%) in accordance with no treatment (Fig. 6f). Following pretreatment with **6a** and **6e**, the protein expression levels of SOD2 were significantly increased (86.77 ± 5.49% and 88.27 ± 5.79%) compared with the H_2O_2 treatment and greater than the resveratrol (81.4 ± 2.07%). The association of chalcone hybrids and AD progression is also supported by both *in vitro* and *in vivo* models.

Chalcone-O-alkylamine and -O-carbamate derivatives displayed good antioxidant activity, inhibited $A\beta_{1-42}$ aggregation, and provided neuroprotective effect against H_2O_2-induced PC12 cell (14) as well as xanthohumol from hops and chalcone analogues revealed an up-regulation of antioxidant genes through Kelch-like ECH-associated protein 1 (Keap1)/Nuclear factor erythroid 2-related factor 2 (Nrf2)/antioxidant response element (ARE) enhancement in PC12 cells (13, 17, 29). Therefore, the presence of chalcone-triazole derivatives (**6a** and **6e)** attenuated H_2O_2-induced neuronal damage by a reduction of the excessive ROS. In view of structural feature, presumably, the α, β-unsaturated keto group (electrophilic center) of **6a** and **6e** could mimic the SOD activity by interacting with the ROS leading to the significant increase level of SOD2 protein. Phenolic compound bearing aldehyde group was also reported to upregulate the SOD2 protein level (58). In addition, the 1,2,3-triazole scaffold of the compounds may exhibit bio-metal chelating effect, which could protect against the intracellular ROS formation (8).

*2.2.6 Involvement of the SIRT1/2/3-FOXO3a pathway by **6a** and **6e** exhibits neuroprotection in H_2O_2-treated SH-SY5Y cells*

Sirtuin (SIRT) family is well known to confer resistance of cells to oxidative stress, longevity, DNA damage repair, mitochondrial function, and metabolism (61, 62). Apart from this, SIRT1, SIRT2, and SIRT3 have also been found to mediate beneficial effects in neurological diseases. SIRT1 is mainly localized in the nucleus of the cells, SIRT2 is found in the cytoplasm, and SIRT3 is predominant in the mitochondria. Several oxidative stress models were shown to decrease the excessive ROS in part due to the activation of SIRT1 and SIRT3, whereas inhibit SIRT2. This mechanism is highlighted through the SIRT1/2/3-FOXO3a pathway in which the transcription factor mitochondrial FOXO3a became upregulated and further stimulated downstream antioxidant enzymes (SOD2 and CAT) to detoxify ROS and promote DNA repairing (63, 64). Moreover, FOXO3a requires SIRT deacetylase activity for its transcriptional protection of cell death from the oxidative damage (61, 65).

The well-known SIRT1 activator, resveratrol, was administered to determine its biological properties on several *in vitro* and *in vivo* models. The neuroprotection afforded by resveratrol against oxidative stress was reported as a robust candidate for AD therapeutic

according to its abilities for preventing Aβ accumulation, attenuating tau aggregation, enhancing antioxidant defense, reciprocally reducing inflammation and decreasing cytotoxicity through SIRT family (62, 66). Further investigation into SIRT1, SIRT2, and SIRT3 roles may provide promising molecular targets underlying neurodegenerative disorders.

In order to understand whether the modulation of SIRT pathway by **6a** and **6e** was related to neuroprotective effect, the protein expressions of SIRT1, SIRT2, SIRT3, and FOXO3a were examined by Western blotting. As illustrated in Fig. 6c-6g, H_2O_2 treatment exhibited the reduction of SIRT1, SIRT3, FOXO3a (59.75 ± 3.68%, 41.93 ± 2.94%, 60.58 ± 4.47%, respectively) and the induction of SIRT2 protein levels (134.50 ± 6.04%) compared to the control. However, no obvious differences were identified in the SIRT1, SIRT2, SIRT3, and FOXO3a between the untreated cells and compounds **6a** and **6e**-pretreated cells. By contrast, the decreased levels of SIRT1, SIRT3, and FOXO3a proteins caused by H_2O_2 were markedly improved by pretreatments with **6a** (SIRT1; 90.52 ± 8.20%, SIRT3; 76.48 ± 3.96%, and FOXO3a; 87.17 ± 7.19%, respectively) and **6e** (SIRT1; 91.51 ± 2.04%, SIRT3; 68.0 ± 3.09%, and FOXO3a; 88.93 ± 4.58%, respectively), while SIRT2 protein was reduced by **6a** (111.60 ± 5.18%) and **6e** pretreatments (99.25 ± 2.44%), in accordance with the H_2O_2 alone. Particularly, **6a** and **6e** demonstrated slightly stronger effects on SIRT1 protein expression compared with the resveratrol (90.03 ± 4.62%), whereas the levels of SIRT2, SIRT3, and FOXO3a protein expressions by resveratrol pretreatment were more potent than **6a** and **6e** (94.50 ± 5.43%, 85.64 ± 4.21%, and 94.13 ± 2.90%, respectively). The resveratrol has been highlighted to influence mitochondrial biogenesis, cytoprotection, amyloid aggregation, and ROS production via activating SIRT1 (4). Similar to the previous studies, butein and isoliquiritigenin are natural chalcones found in *Hydnophytum formicarum* Jack. Both compounds were considered to be used as an alternative AD treatment, which promoted SIRT1 and a disintegrin and metalloproteinase domain-containing protein 10 (ADAM10) activities in modulation of Aβ shedding and attenuation of neuronal cell death (55, 67). Another model of oxidative stress mediated by $A\beta_{1-42}$ against human fetal neurons was reported that phenol–triazole ligands can target multiple factors associated with AD comprising antioxidant capacity, copper-binding affinity, interaction and modulation of Aβ peptide aggregation (68) as well as anti-aggregation towards $A\beta_{1-42}$ and anticholinesterase activities by 2-arylbenzofuran derivative bearing a substituted triazole (69). These results

indicated that chalcone-triazole hybrids **6a** and **6e** display anti-neurodegenerative effects by modulation of the SIRT1/2/3-FOXO3a signaling pathway.

In conclusion, the data demonstrated that chalcone-triazole derivatives-treated neuronal cells maintain anti-apoptotic, cellular antioxidant status, and mitochondrial function without neurotoxicity. Moreover, these pretreatments also completely protect the neurons against H_2O_2-mediated oxidative damage through SIRT1/2/3-FOXO3a signaling pathway (Fig. 7). Notably, the alternative strategy for the design of novel neuroprotective compounds equivalent to the well-known antioxidant (resveratrol) was provided. Thus, chalcone-triazole derivatives could be developed as lead candidates in the prevention or treatment of neurodegenerative diseases.

3. Experimental

3.1 General

Column chromatography was carried out using silica gel 60 (70-230 mesh ASTM). Analytical thin-layer chromatography (TLC) was performed on silica gel 60 F_{254} aluminum sheets. ^{1}H- and ^{13}C-NMR spectra were recorded on a Bruker AVANCE 300 NMR spectrometer (operating at 300 MHz for ^{1}H and 75 MHz for ^{13}C). FTIR spectra were obtained using a universal attenuated total reflectance attached on a Perkin–Elmer Spectrum One spectrometer. High resolution mass spectra (HRMS) were recorded on a Bruker Daltonics (microTOF). Melting points were determined using a Griffin melting point apparatus and were uncorrected.

*3.2 Synthesis of (E)-1-(4-aminophenyl)-3-(3,4-dimethoxyphenyl)prop-2-en-1-one (**3**)* (70)

To a mixture of 3,4-dimethoxybenzaldehyde **1** (6 mmol) and 4-aminoacetophenone **2** (6 mmol) in ethanol (15 mL) was stirred at 4 ^{o}C, then 40% KOH (5 mL) was added dropwise, and stirred at room temperature for 4 h. The reaction mixture was neutralized with 2M HCl, then the precipitate was filtered, washed with cold water and recrystallized from ethanol to give compound **3**.

Yellow solid. 85%. mp 121-122 ^{o}C. IR (UATR) cm^{-1}: 3456, 3360, 3232, 1628, 1598, 1510. ^{1}H NMR (300 MHz, DMSO-d_6) δ 3.79 (s, 3H, OCH_3), 3.84 (s, 3H, OCH_3), 6.09 (s, 2H, NH_2), 6.61 (d, *J* = 8.6 Hz, 2H, C3-Ar*H* and C5-Ar*H*), 6.98 (d, *J* = 8.3 Hz, 1H, C5′-Ar*H*), 7.30 (d, *J* = 8.2 Hz, 1H, C6′-Ar*H*), 7.47 (s, 1H, C2′-Ar*H*), 7.56 (d, *J* = 15.4 Hz, 1H, CH=C*H*CO), 7.74 (d, *J* = 15.4 Hz, 1H, C*H*=CHCO), 7.92 (d, *J* = 8.6 Hz, 2H, C2-Ar*H* and C6-Ar*H*). ^{13}C NMR (75 MHz,

DMSO-d_6) δ 56.1, 56.2, 111.0, 112.1, 113.2, 120.5, 123.7, 126.1, 128.5, 131.5, 142.3, 149.5, 151.2, 154.1, 186.4. HRMS-TOF: m/z $[M + H]^+$ 284.1293 (Calcd for $C_{17}H_{18}NO_3$: 284.1281).

3.3 Synthesis of (E)-1-(4-azidophenyl)-3-(3,4-dimethoxyphenyl)prop-2-en-1-one (4)

To a cold solution of aminochalcone **3** (3 mmol) in HCl:CH_3COOH (3:3 mL) at 0 °C, a solution of sodium nitrite (9 mmol) in water (5 mL) was added. The stirred reaction mixture was maintained for 15 min and then added dropwise a solution of sodium azide (9 mmol) in water (5 mL). The reaction mixture was allowed to stir at room temperature for 0.5 h, then the precipitate was filtered, washed with cold water and recrystallized from methanol to provide compound **4**.

Yellow solid. 77%. mp 120-121 °C. IR (UATR) cm^{-1}: 2124, 1655, 1598, 1510. ^1H NMR (300 MHz, $CDCl_3$) δ 3.92 (s, 3H, OC*H*$_3$), 3.93 (s, 3H, OC*H*$_3$), 6.88 (d, *J* = 8.3 Hz, 1H, C5′-Ar*H*), 7.11 (d, *J* = 8.6 Hz, 2H, C3-Ar*H* and C5-Ar*H*), 7.13 (d, *J* = 1.5 Hz, 1H, C2′-Ar*H*), 7.24 (dd, *J* = 8.3, 1.5 Hz, 1H, C6′-Ar*H*), 7.35 (d, *J* = 15.6 Hz, 1H, CH=C*H*CO), 7.75 (d, *J* = 15.6 Hz, 1H, C*H*=CHCO), 8.02 (d, *J* = 8.6 Hz, 2H, C2-Ar*H* and C6-Ar*H*). ^{13}C NMR (75 MHz, $CDCl_3$) δ 56.0, 110.2, 111.2, 119.0, 119.5, 123.2, 127.8, 130.4, 135.1, 144.5, 145.1, 149.3, 151.5, 188.8. HRMS-TOF: m/z $[M + H]^+$ 310.1191 (Calcd for $C_{17}H_{16}N_3O_3$: 310.1186).

*3.4 General procedure for the synthesis of propynyloxy derivatives (**5a-g**)*

A propargyl bromide (2.4 mmol) was added to a suspension of an appropiate phenol (2 mmol) and potassium carbonate (4 mmol) in acetone (15 mL). The suspension was heated under reflux for 2 h. The reaction was allowed to cool and then concentrated under reduced pressure. Water (30 mL) was added and extracted with EtOAc (3 × 30 mL). The organic extracts were combined and washed with water (20 mL) and brine (20 mL). The organic layer was dried over anhydrous sodium sulfate, filtered and concentrated *in vacuo*. The crude product was purified by column chromatography. ^1H NMR spectra of (2-propynyloxy)benzene (**5a**) (71), 1-methyl-4-(2-propynyloxy)benzene (**5b**) (72), 1-methyl-2-(2-propynyloxy)benzene (**5c**) (73), methyl 2-(2-propynyloxy)benzoate (**5d**) (74), 4-(2-propynyloxy)benzaldehyde (**5e**) (75), 4-methoxy-3-(2-propynyloxy)benzaldehyde (**5f**) (76), and 2-(2-propynyloxy)naphthalene (**5g**) (77) were consistent with those reported in the literatures.

*3.5 General procedure for the synthesis of chalcone-triazole derivatives (**6a-g**)*

To a stirred solution of azidochalcone **4** (0.2 mmol) and alkyne **5** (0.22 mmol) in *t*-BuOH:H_2O (3:3 mL), $CuSO_4 \cdot 5H_2O$ (0.22 mmol) and sodium ascorbate (0.5 mmol) were added. The reaction mixture was stirred at room temperature for 2 h and then concentrated under reduced pressure. The residue was added water (10 mL) and extracted with dichloromethane (3 × 20 mL). The combined organic phases were washed with water (20 mL), dried over anhydrous sodium sulfate and evaporated to dryness. The crude product was purified using silica gel column chromatography and eluted with methanol:dichloromethane (1:50) to give compounds **6a-g**.

*3.5.1 (E)-3-(3,4-dimethoxyphenyl)-1-(4-(4-(phenoxymethyl)-1H-1,2,3-triazol-1-yl)phenyl)prop-2-en-1-one (**6a**)*

Pale yellow solid. 78% yield. mp 173-174 °C. IR (UATR) cm^{-1}: 1656, 1584, 1513. ^1H NMR (300 MHz, DMSO-d_6) δ 3.83 (s, 3H, OCH_3), 3.88 (s, 3H, OCH_3), 5.27 (s, 2H, CH_2O), 6.98 (t, *J* = 7.3 Hz, 1H, Ar*H*), 7.04 (d, *J* = 8.4 Hz, 1H, Ar*H*), 7.09 (d, *J* = 8.3 Hz, 2H, Ar*H*), 7.33 (t, *J* = 7.9 Hz, 2H, Ar*H*), 7.44 (d, *J* = 8.2 Hz, 1H, Ar*H*), 7.58 (s, 1H, Ar*H*), 7.76 (d, *J* = 15.5 Hz, 1H, CH=C*H*CO), 7.90 (d, *J* = 15.5 Hz, 1H, C*H*=CHCO), 8.14 (d, *J* = 8.6 Hz, 2H, Ar*H*), 8.38 (d, *J* = 8.6 Hz, 2H, Ar*H*), 9.14 (s, 1H, C*H*N). ^{13}C NMR (75 MHz, DMSO-d_6) δ 56.1, 56.3, 61.4, 111.5, 112.1, 115.2, 119.8, 120.4, 121.5, 123.5, 124.7, 127.9, 130.0, 130.8, 138.0, 139.8, 144.8, 145.6, 149.5, 152.0, 158.4, 188.3. HRMS-TOF: m/z $[M + Na]^+$ 464.1581 (Calcd for $C_{26}H_{23}N_3NaO_4$: 464.1569).

*3.5.2 (E)-3-(3,4-dimethoxyphenyl)-1-(4-(4-((p-tolyloxy)methyl)-1H-1,2,3-triazol-1-yl)phenyl)prop-2-en-1-one (**6b**)*

Pale yellow solid. 89% yield. mp 178-179 °C. IR (UATR) cm^{-1}: 1654, 1604, 1583, 1510. ^1H NMR (300 MHz, DMSO-d_6) δ 2.24 (s, 3H, CH_3), 3.83 (s, 3H, OCH_3), 3.87 (s, 3H, OCH_3), 5.22 (s, 2H, CH_2O), 6.97 (d, *J* = 8.4 Hz, 2H, Ar*H*), 7.05 (d, *J* = 8.3 Hz, 1H, Ar*H*), 7.12 (d, *J* = 8.5 Hz, 2H, Ar*H*), 7.44 (d, *J* = 8.4 Hz, 1H, Ar*H*), 7.58 (s, 1H, Ar*H*), 7.75 (d, *J* = 15.4 Hz, 1H, CH=C*H*CO), 7.90 (d, *J* = 15.5 Hz, 1H, C*H*=CHCO), 8.14 (d, *J* = 8.5 Hz, 2H, Ar*H*), 8.38 (d, *J* = 8.6 Hz, 2H, Ar*H*), 9.12 (s, 1H, C*H*N). ^{13}C NMR (75 MHz, DMSO-d_6) δ 20.5, 56.1, 56.3, 61.5, 111.5, 112.1, 115.1, 119.8, 120.4, 123.4, 124.7, 127.9, 130.2, 130.4, 130.8, 138.0, 139.8, 144.9, 145.6, 149.5, 152.0, 156.3, 188.3. HRMS-TOF: m/z $[M + Na]^+$ 478.1737 (Calcd for $C_{27}H_{25}N_3NaO_4$: 478.1726).

*3.5.3 (E)-3-(3,4-dimethoxyphenyl)-1-(4-(4-((o-tolyloxy)methyl)-1H-1,2,3-triazol-1-yl)phenyl)prop-2-en-1-one (**6c**)*

Pale yellow solid. 87% yield. mp 159-160 °C. IR (UATR) cm^{-1}: 1654, 1590, 1515. ^1H NMR (300 MHz, DMSO-d_6) δ 2.16 (s, 3H, CH_3), 3.82 (s, 3H, OCH_3), 3.86 (s, 3H, OCH_3), 5.26 (s, 2H, CH_2O), 6.82-6.92 (m, 1H, Ar*H*), 7.03 (d, *J* = 8.3 Hz, 1H, Ar*H*), 7.13-7.20 (m, 3H, Ar*H*), 7.42 (dd, *J* = 8.4, 1.7 Hz, 1H, Ar*H*), 7.56 (d, *J* = 1.7 Hz, 1H, Ar*H*), 7.75 (d, *J* = 15.5 Hz, 1H, CH=C*H*CO), 7.88 (d, *J* = 15.5 Hz, 1H, C*H*=CHCO), 8.14 (d, *J* = 8.7 Hz, 2H, Ar*H*), 8.36 (d, *J* = 8.6 Hz, 2H, Ar*H*), 9.10 (s, 1H, C*H*N). ^{13}C NMR (75 MHz, DMSO-d_6) δ 16.5, 56.1, 56.3, 61.7, 111.5, 112.1, 112.4, 119.9, 120.4, 121.3, 123.3, 124.6, 126.5, 127.4, 127.9, 130.8, 131.0, 138.0, 139.8, 145.1, 145.6, 149.5, 152.0, 156.6, 188.4. HRMS-TOF: m/z $[M + Na]^+$ 478.1737 (Calcd for $C_{27}H_{25}N_3NaO_4$: 478.1724).

3.5.4 (E)-methyl2-((1-(4-(3-(3,4-dimethoxyphenyl)acryloyl)phenyl)-1H-1,2,3-triazol-4-yl)methoxy)benzoate ***(6d)***

Pale yellow solid. 73% yield.mp 163-164 °C. IR (UATR) cm^{-1}: 1719, 1661, 1593, 1520. ^1H NMR (300 MHz, DMSO-d_6) δ 3.76 (s, 3H, COCH_3), 3.82 (s, 3H, OCH_3), 3.87 (s, 3H, OCH_3), 5.35 (s, 2H, CH_2O), 7.00-7.11 (m, 2H, Ar*H*), 7.37-7.47 (m, 2H, Ar*H*), 7.53-7.61 (m, 2H, Ar*H*), 7.67 (dd, *J* = 7.7, 1.7 Hz, 1H, Ar*H*), 7.77 (d, *J* = 15.5 Hz, 1H, CH=C*H*CO), 7.89 (d, *J* = 15.5 Hz, 1H, C*H*=CHCO), 8.13 (d, *J* = 8.8 Hz, 2H, Ar*H*), 8.38 (d, *J* = 8.8 Hz, 2H, Ar*H*), 9.06 (s, 1H, C*H*N). ^{13}C NMR (75 MHz, DMSO-d_6) δ 52.4, 56.1, 56.2, 62.6, 111.4, 112.1, 115.0, 119.8, 120.4, 121.4, 123.4, 124.7, 127.9, 130.8, 131.2, 134.0, 138.0, 139.8, 144.6, 145.7, 149.5, 152.0, 157.3, 166.5, 188.4. HRMS-TOF: m/z $[M + Na]^+$ 522.1636 (Calcd for $C_{28}H_{25}N_3NaO_6$: 522.1632).

3.5.5 (E)-4-((1-(4-(3-(3,4-dimethoxyphenyl)acryloyl)phenyl)-1H-1,2,3-triazol-4-yl)methoxy)benzaldehyde ***(6e)***

Pale yellow solid. 82% yield. mp 149-150 °C. IR (UATR) cm^{-1}: 1688, 1655, 1602, 1581, 1509. ^1H NMR (300 MHz, DMSO-d_6) δ 3.82 (s, 3H, OCH_3), 3.87 (s, 3H, OCH_3), 5.41 (s, 2H, CH_2O), 7.03 (d, *J* = 8.4 Hz, 1H, Ar*H*), 7.29 (d, *J* = 8.7 Hz, 2H, Ar*H*), 7.42 (dd, *J* = 8.4, 1.7 Hz, 1H, Ar*H*), 7.56 (d, *J* = 1.7 Hz, 1H, Ar*H*), 7.75 (d, *J* = 15.5 Hz, 1H, CH=C*H*CO), 7.88 (d, *J* = 15.5 Hz, 1H, C*H*=CHCO), 7.89 (d, *J* = 8.8 Hz, 2H, Ar*H*), 8.13 (d, *J* = 8.7 Hz, 2H, Ar*H*), 8.37 (d, *J* = 8.7 Hz, 2H, Ar*H*), 9.14 (s, 1H, C*H*N), 9.89 (s, 1H, C*H*O). ^{13}C NMR (75 MHz, DMSO-d_6) δ 56.1, 56.3, 61.8, 111.4, 112.1, 115.7, 119.8, 120.5, 123.8, 124.7, 127.9, 130.5, 130.8, 132.3, 138.1, 139.8, 144.1, 145.7, 149.5, 152.0, 163.3, 188.4, 191.9. HRMS-TOF: m/z $[M + Na]^+$ 492.1523 (Calcd for $C_{27}H_{23}N_3NaO_5$: 492.1523).

*3.5.6 (E)-3-((1-(4-(3-(3,4-dimethoxyphenyl)acryloyl)phenyl)-1H-1,2,3-triazol-4-yl)methoxy)-4-methoxybenzaldehyde (**6f**)*

Pale yellow solid. 83% yield. mp 151-152 °C. IR (UATR) cm^{-1}: 1683, 1658, 1593, 1511. ^1H NMR (300 MHz, DMSO-d_6) δ 3.83 (s, 3H, OCH_3), 3.87 (s, 6H, 2 × OCH_3), 5.34 (s, 2H, CH_2O), 7.04 (d, *J* = 8.4 Hz, 1H, Ar*H*), 7.22 (d, *J* = 8.3 Hz, 1H, Ar*H*), 7.43 (d, *J* = 7.3 Hz, 1H, Ar*H*), 7.57 (s, 1H, Ar*H*), 7.61 (d, *J* = 8.3 Hz, 1H, Ar*H*), 7.67 (s, 1H, Ar*H*), 7.74 (d, *J* = 15.4 Hz, 1H, CH=C*H*CO), 7.89 (d, *J* = 15.4 Hz, 1H, C*H*=CHCO), 8.14 (d, *J* = 8.6 Hz, 2H, Ar*H*), 8.37 (d, *J* = 8.6 Hz, 2H, Ar*H*), 9.12 (s, 1H, C*H*N), 9.87 (s, 1H, C*H*O). ^{13}C NMR (75 MHz, DMSO-d_6) δ 56.1, 56.3, 56.4, 62.1, 111.5, 112.1, 112.2, 112.4, 119.9, 120.4, 123.8, 124.6, 126.9, 127.9, 130.1, 130.8, 138.1, 139.8, 144.3, 145.6, 148.3, 149.5, 152.0, 155.0, 188.4, 191.8. HRMS-TOF: m/z $[M + Na]^+$ 522.1640 (Calcd for $C_{28}H_{25}N_3NaO_6$: 522.1641).

*3.5.7 (E)-3-(3,4-dimethoxyphenyl)-1-(4-(4-((naphthalen-2-yloxy)methyl)-1H-1,2,3-triazol-1-yl)phenyl)prop-2-en-1-one (**6g**)*

Pale yellow solid. 89% yield. mp 190-191 °C. IR (UATR) cm^{-1}: 1654, 1601, 1512. ^1H NMR (300 MHz, DMSO-d_6) δ 3.83 (s, 3H, OCH_3), 3.88 (s, 3H, OCH_3), 5.40 (s, 2H, CH_2O), 7.05 (d, *J* = 8.4 Hz, 1H, Ar*H*), 7.25 (dd, *J* = 8.9, 2.4 Hz, 1H, Ar*H*), 7.34-7.60 (m, 5H, Ar*H*), 7.75 (d, *J* = 15.5 Hz, 1H, CH=C*H*CO), 7.80-7.95 (m, 4H, Ar*H* and C*H*=CHCO), 8.15 (d, *J* = 8.7 Hz, 2H, Ar*H*), 8.39 (d, *J* = 8.6 Hz, 2H, Ar*H*), 9.20 (s, 1H, C*H*N). ^{13}C NMR (75 MHz, DMSO-d_6) δ 56.1, 56.3, 61.6, 107.8, 111.5, 112.1, 119.1, 119.8, 120.4, 123.6, 124.3, 124.7, 127.0, 127.3, 127.9, 128.0, 129.2, 129.9, 130.8, 134.7, 138.0, 139.9, 144.7, 145.6, 149.5, 152.0, 156.3, 188.3. HRMS-TOF: m/z $[M + Na]^+$ 514.1737 (Calcd for $C_{30}H_{25}N_3NaO_4$: 514.1720).

3.6 Biological activity

3.6.1 Chemical and reagents

3-(4,5-Dimethylthiazol-2-yl)-2,5-diphenyl tetrazolium bromide (MTT) and 2',7′-dichlorofluorescein diacetate (DCFDA) were obtained from Molecular Probes (Eugene, OR, USA). Annexin V & Dead Cell Assay Kit and Immobilon ECL Ultra Western HRP Substrate were purchased from Merck Millipore (Darmstadt, Germany). Protease inhibitor cocktail were obtained from Calbiochem (Cambridge, MA, USA). RIPA and primary antibodies including anti-BAX, BCL-2, SIRT1, SIRT2, SIRT3, FOXO3a, SOD2, and β-actin as well as secondary antibodies were supplied from Cell Signaling Technology (Beverly, MA, USA).

All chemical reagents used in this experiment were analytical grade from Sigma (St. Louis, MO, USA).

3.6.2 Cytotoxicity assay

Green Fluorescent Protein (GFP) detection method was conducted to determine cytotoxicity (78). The GFP-expressing Vero cell line was produced in-house by transfection of African green monkey kidney cell line (Vero, ATCC CCL-81) with pEGFP-N1 plasmid (Clontech). Minimal essential medium supplemented with 10% heat-inactivated fetal bovine serum (FBS), 1 mM sodium pyruvate, 2 mM L-glutamine, 0.8 mg/mL geneticin, and 1.5 g/L sodium bicarbonate were utilized to culture the cell line. 45 µL of cell suspension at 3.3×10^4 cells/mL was added into to 384-well plates with 5 µL of chalcone-triazole derivatives or ellipticine formerly diluted in 0.5% DMSO followed by 37 ^oC incubation for 4 days with 5% CO_2. SpectraMax M5 microplate reader (Molecular Devices, USA) was used to detect fluorescence signals with excitation and emission wavelengths of 485 and 535 nm, respectively. Fluorescence signal at day 4 was subtracted with background fluorescence at day 0. The values of IC_{50} values were obtained from dose-response curves with 6 concentrations of 3-fold serially diluted samples using the SOFTMax Pro software (Molecular device). 0.5% DMSO and ellipticine were negative and positive controls, respectively.

3.6.3 Cell viability by MTT assay

SH-SY5Y cell line (human neuroblastoma) obtained from American Type Culture Collection (ATCC) (Manassas, VA, USA) was utilized in this work. Dulbecco's Modified Eagle Medium (DMEM), 1% penicillin-streptomycin, and 10% heat-inactivated fetal bovine serum (FBS) from Gibco BRL (Gaithersburg, MD, USA) were used to culture SH-SY5Y cells in 75-cm^2 flasks at 37°C with 5% CO_2. Next, for testing the effect of all compounds on cell viability, the cells were grown in 96-well plates for 24 h until reaching 80% confluence, then various concentrations of chalcone-triazole derivatives or resveratrol (0.1-100 µM) were added in the plates for 3 h, followed by incubation with 400 µM H_2O_2 or 10 µM $A\beta_{1-42}$ oligomer. Subsequently, 5 mg/mL of MTT was included in all wells followed by incubation for 3 h at 37 °C. Upon MTT removal, an extraction buffer (0.04 N HCl in isopropanol) was applied to each well. The resulting purple formazan was measured by microplate reader (BioTek Instruments, VT, USA) at 570 nm.

3.6.4 Cell apoptosis by Flow cytometry

For evaluation of cell apoptosis, 6-well plates were used for seeding SH-SY5Y cells, and 1 μM of chalcone-triazole derivatives or resveratrol was added in the wells for 3 h, followed by 24 h incubation with 400 μM H_2O_2. Following the incubation, the cells were harvested and determined apoptosis profiles using Annexin V & Dead Cell Assay Kit. Muse™ cell analyzer (Merck Millipore, USA) was utilized for analyzing the percentages of living, apoptotic, and dead cells.

3.6.5 Mitochondrial membrane potential by rhodamine staining

Mitochondrial membrane potential was determined by rhodamine 123. After the treatment, cells were washed twice with PBS, followed by incubation with 10 μM rhodamine 123 at 37°C for 30 min. Emission spectra at 488 nm and excitation spectra at 525 nm were measured by microplate reader and imaged by fluorescence microscope.

3.6.6 Intracellular ROS levels by DCFDA assay

The cells were treated as described above and stained with 10 μM DCFDA for 30 min in the dark. The fluorescence signals within the cells were measured using microplate reader at excitation and emission spectra of 495 nm and 527 nm, respectively and visualized by fluorescence microscope.

3.6.7 Western blot analysis

Following pretreatment with chalcone-triazole derivatives or resveratrol, SH-SY5Y cells were lysed in the RIPA lysis buffer. Based on the protein concentration measured by the Bradford assay, 20 μg of samples were run on sodium dodecyl sulphate-polyacrylamide gels and electrotransferred to polyvinylidene difluoride (PVDF) membranes. After blocking with 5% skimmed milk in Tris-buffer containing 0.1% Tween-20 (TBST) for 2 h, the primary antibodies (SIRT1, SIRT2, SIRT3, FOXO3a, BAX, BCL-2, and SOD2) were applied for overnight incubation at 4°C. Next, the blots were added with horseradish peroxidase-conjugated secondary antibodies incubated at room temperature for an hour, then the membrane was developed using ECL.The protein levels of all bands were determined using ChemiDoc™ MP Imaging System and Image Lab Software (Bio-Rad Laboratories, Inc, Hercules, CA, USA) and normalized to β-actin.

3.6.8 Statistical analysis

Statistical analysis was performed using GraphPad Prism 6 software (GraphPad Software Inc.) and one-way ANOVA followed by a Tukey-Kramer post-test was employed for comparisons among three or more groups. Data were expressed as mean ± S.E.M. values

from three independent experiments. A p-value less than 0.05 was set as statistically significant.

Acknowledgments

This project is supported by the research grants from Srinakharinwirot University (grant no. 085/2563). We are indebted to Chulabhorn Research Institute for recording mass spectra.

References

1. Liu YG, Li X, Xiong DC, Yu B, Pu X, Ye XS. Synthetic phenylethanoid glycoside derivatives as potent neuroprotective agents. Eur J Med Chem. 2015;95:313-23.
2. Zanforlin E, Zagotto G, Ribaudo G. The medicinal chemistry of natural and semisynthetic compounds against Parkinson's and Huntington's diseases. ACS Chem Neurosci. 2017;8(11):2356-68.
3. Iqbal S, Shah FA, Naeem K, Nadeem H, Sarwar S, Ashraf Z, et al. Succinamide derivatives ameliorate neuroinflammation and oxidative stress in scopolamine-induced neurodegeneration. Biomolecules 2020;10(3):443.
4. Wąsik A, Antkiewicz Michaluk L. The mechanism of neuroprotective action of natural compounds. Pharmacol Rep 2017;69(5):851-60.
5. Bansal R, Singh R. Exploring the potential of natural and synthetic neuroprotective steroids against neurodegenerative disorders: A literature review. Medicinal research reviews. 2018;38(4):1126-58.
6. Zhuang C, Zhang W, Sheng C, Zhang W, Xing C, Miao Z. Chalcone: A privileged structure in medicinal chemistry. Chem Rev. 2017;117(12):7762-810.
7. Gomes MN, Muratov EN, Pereira M, Peixoto JC, Rosseto LP, Cravo PVL, et al. Chalcone derivatives: Promising starting points for drug design. Molecules (Basel, Switzerland). 2017;22(8):1210.
8. Bozorov K, Zhao J, Aisa HA. 1,2,3-Triazole-containing hybrids as leads in medicinal chemistry: A recent overview. Bioorg Med Chem. 2019;27(16):3511-31.
9. Dheer D, Singh V, Shankar R. Medicinal attributes of 1,2,3-triazoles: Current developments. Bioorg Chem. 2017;71:30-54.

10. Sahu NK, Balbhadra SS, Choudhary J, Kohli DV. Exploring pharmacological significance of chalcone scaffold: A review. Curr Med Chem. 2012;19(2):209-25.
11. Daniela Ilieva B, Iva Todorova T. Trends in utilization of the pharmacological potential of chalcones. Curr Clin Pharmacol. 2010;5(1):1-29.
12. Zhang X, Rakesh KP, Bukhari SNA, Balakrishna M, Manukumar HM, Qin HL. Multi-targetable chalcone analogs to treat deadly Alzheimer's disease: Current view and upcoming advice. Bioorg Chem. 2018;80:86-93.
13. De Freitas Silva M, Pruccoli L, Morroni F, Sita G, Seghetti F, Viegas Jr C, et al. The Keap1/Nrf2-ARE pathway as a pharmacological target for chalcones. Molecules (Basel, Switzerland). 2018;23(7).
14. Bai P, Wang K, Zhang P, Shi J, Cheng X, Zhang Q, et al. Development of chalcone-O-alkylamine derivatives as multifunctional agents against Alzheimer's disease. Eur J Med Chem. 2019;183:111737.
15. Sang Z, Wang K, Zhang P, Shi J, Liu W, Tan Z. Design, synthesis, *in-silico* and biological evaluation of novel chalcone derivatives as multi-function agents for the treatment of Alzheimer's disease. Eur J Med Chem. 2019;180:238-52.
16. Sang Z, Wang K, Shi J, Liu W, Tan Z. Design, synthesis, *in-silico* and biological evaluation of novel chalcone-O-carbamate derivatives as multifunctional agents for the treatment of Alzheimer's disease. Eur J Med Chem. 2019;178:726-39.
17. Wu JZ, Cheng CC, Shen LL, Wang ZK, Wu SB, Li WL, et al. Synthetic chalcones with potent antioxidant ability on H_2O_2-induced apoptosis in PC12 cells. Int J Mol Sci 2014;15(10):18525-39.
18. Jiwrajka M, Phillips A, Butler M, Rossi M, Pocock JM. The plant-derived chalcone 2,2',5'-trihydroxychalcone provides neuroprotection against toll-like receptor 4 triggered inflammation in microglia. Oxid Med Cell Longev. 2016;2016:6301712.
19. Cong L, Dong X, Wang Y, Deng Y, Li B, Dai R. On the role of synthesized hydroxylated chalcones as dual functional amyloid-β aggregation and ferroptosis inhibitors for potential treatment of Alzheimer's disease. Eur J Med Chem. 2019;166:11-21.
20. Xiao G, Li Y, Qiang X, Xu R, Zheng Y, Cao Z, et al. Design, synthesis, and biological evaluation of 4′-aminochalcone-rivastigmine hybrids as multifunctional agents for the treatment of Alzheimer's disease. Bioorg Med Chem. 2017;25(3):1030-41.

21. Jeon KH, Lee E, Jun KY, Eom JE, Kwak SY, Na Y, et al. Neuroprotective effect of synthetic chalcone derivatives as competitive dual inhibitors against μ-calpain and cathepsin B through the downregulation of tau phosphorylation and insoluble Aβ peptide formation. Eur J Med Chem. 2016;121:433-44.

22. Liu Hr, Huang Xq, Lou Dh, Liu Xj, Liu Wk, Wang Qa. Synthesis and acetylcholinesterase inhibitory activity of Mannich base derivatives flavokawain B. Bioorg Med Chem Lett. 2014;24(19):4749-53.

23. Kang L, Gao XH, Liu HR, Men X, Wu HN, Cui PW, et al. Structure-activity relationship investigation of coumarin-chalcone hybrids with diverse side-chains as acetylcholinesterase and butyrylcholinesterase inhibitors. Mol Divers. 2018;22(4):893-906.

24. Rampa A, Bartolini M, Pruccoli L, Naldi M, Iriepa I, Moraleda I, et al. Exploiting the chalcone scaffold to develop multifunctional agents for Alzheimer's disease. Molecules (Basel, Switzerland). 2018;23(8).

25. Burmaoglu S, Yilmaz AO, Polat MF, Kaya R, Gulcin İ, Algul O. Synthesis and biological evaluation of novel tris-chalcones as potent carbonic anhydrase, acetylcholinesterase, butyrylcholinesterase and α-glycosidase inhibitors. Bioorg Chem. 2019;85:191-7.

26. Jung JC, Jang S, Lee Y, Min D, Lim E, Jung H, et al. Efficient synthesis and neuroprotective effect of substituted 1,3-diphenyl-2-propen-1-ones. J Med Chem. 2008;51(13):4054-8.

27. Kühnl J, Roggenkamp D, Gehrke SA, Stäb F, Wenck H, Kolbe L, et al. Licochalcone A activates Nrf2 *in vitro* and contributes to licorice extract-induced lowered cutaneous oxidative stress *in vivo*. Exp Dermatol. 2015;24(1):42-7.

28. Kim SS, Lim J, Bang Y, Gal J, Lee SU, Cho YC, et al. Licochalcone E activates Nrf2/antioxidant response element signaling pathway in both neuronal and microglial cells: therapeutic relevance to neurodegenerative disease. J Nutr Biochem. 2012;23(10):1314-23.

29. Yao J, Zhang B, Ge C, Peng S, Fang J. Xanthohumol, a polyphenol chalcone present in hops, activating Nrf2 enzymes to confer protection against oxidative damage in PC12 cells. J Agric Food Chem. 2015;63(5):1521-31.

30. Xu Z, Zhao SJ, Liu Y. 1,2,3-Triazole-containing hybrids as potential anticancer agents: Current developments, action mechanisms and structure-activity relationships. Eur J Med Chem. 2019;183:111700.

31. Jones MR, Dyrager C, Hoarau M, Korshavn KJ, Lim MH, Ramamoorthy A, et al. Multifunctional quinoline-triazole derivatives as potential modulators of amyloid-β peptide aggregation. J Inorg Biochem. 2016;158:131-8.
32. Yazdani M, Edraki N, Badri R, Khoshneviszadeh M, Iraji A, Firuzi O. Multi-target inhibitors against Alzheimer disease derived from 3-hydrazinyl 1,2,4-triazine scaffold containing pendant phenoxy methyl-1,2,3-triazole: Design, synthesis and biological evaluation. Bioorg Chem. 2019;84:363-71.
33. Rastegari A, Nadri H, Mahdavi M, Moradi A, Mirfazli SS, Edraki N, et al. Design, synthesis and anti-Alzheimer's activity of novel 1,2,3-triazole-chromenone carboxamide derivatives. Bioorg Chem. 2019;83:391-401.
34. Jalili Baleh L, Nadri H, Forootanfar H, Samzadeh Kermani A, Küçükkılınç TT, Ayazgok B, et al. Novel 3-phenylcoumarin–lipoic acid conjugates as multi-functional agents for potential treatment of Alzheimer's disease. Bioorg Chem. 2018;79:223-34.
35. Najafi Z, Mahdavi M, Saeedi M, Karimpour Razkenari E, Edraki N, Sharifzadeh M, et al. Novel tacrine-coumarin hybrids linked to 1,2,3-triazole as anti-Alzheimer's compounds: *In vitro* and *in vivo* biological evaluation and docking study. Bioorg Chem 2019;83:303-16.
36. Rani A, Anand A, Kumar K, Kumar V. Recent developments in biological aspects of chalcones: the odyssey continues. Expert Opin Drug Discov. 2019;14(3):249-88.
37. Singh G, Arora A, Kalra P, Maurya IK, Ruizc CE, Estebanc MA, et al. A strategic approach to the synthesis of ferrocene appended chalcone linked triazole allied organosilatranes: Antibacterial, antifungal, antiparasitic and antioxidant studies. Bioorg Med Chem. 2019;27(1):188-95.
38. Singh G, Arora A, Mangat SS, Rani S, Kaur H, Goyal K, et al. Design, synthesis and biological evaluation of chalconyl blended triazole allied organosilatranes as giardicidal and trichomonacidal agents. Eur J Med Chem. 2016;108:287-300.
39. Singh P, Anand A, Kumar V. Recent developments in biological activities of chalcones: A mini review. Eur J Med Chem. 2014;85:758-77.
40. Yadav P, Lal K, Kumar A, Guru SK, Jaglan S, Bhushan S. Green synthesis and anticancer potential of chalcone linked-1,2,3-triazoles. Eur J Med Chem. 2017;126:944-53.
41. Lal K, Yadav P, Kumar A, Kumar A, Paul AK. Design, synthesis, characterization, antimicrobial evaluation and molecular modeling studies of some dehydroacetic acid-chalcone-1,2,3-triazole hybrids. Bioorg Chem. 2018;77:236-44.

42. Pingaew R, Saekee A, Mandi P, Nantasenamat C, Prachayasittikul S, Ruchirawat S, et al. Synthesis, biological evaluation and molecular docking of novel chalcone–coumarin hybrids as anticancer and antimalarial agents. Eur J Med Chem. 2014;85:65-76.
43. Othman SB, Yabe T. Use of hydrogen peroxide and peroxyl radicals to induce oxidative stress in neuronal cells. RAS. 2015;3:40-5.
44. Konyalioglu S, Armagan G, Yalcin A, Atalayin C, Dagci T. Effects of resveratrol on hydrogen peroxide-induced oxidative stress in embryonic neural stem cells. Neural Regen Res. 2013;8(6):485-95.
45. Peritore CS, Ho A, Yamamoto BK, Schaus SE. Resveratrol attenuates L-DOPA-induced hydrogen peroxide toxicity in neuronal cells. Neuroreport. 2012;23(17):989-94.
46. Cline EN, Bicca MA, Viola KL, Klein WL. The amyloid-beta oligomer hypothesis: Beginning of the third decade. J Alzheimers Dis. 2018;64(s1):S567-S610.
47. Cieslik M, Czapski GA, Strosznajder JB. The molecular mechanism of amyloid beta42 peptide toxicity: The role of sphingosine kinase-1 and mitochondrial sirtuins. PLoS One. 2015;10(9):e0137193.
48. Perez de la Cruz V, Korrapati SV, Pedraza-Chaverri J. Redox status and aging link in neurodegenerative diseases. Oxid Med Cell Longev. 2014;2014:270291.
49. Zhang LL, Sui HJ, Liang B, Wang HM, Qu WH, Yu SX, et al. Atorvastatin prevents amyloid-beta peptide oligomer-induced synaptotoxicity and memory dysfunction in rats through a p38 MAPK-dependent pathway. Acta Pharmacol Sin. 2014;35(6):716-26.
50. Giordano CR, Terlecky LJ, Bollig-Fischer A, Walton PA, Terlecky SR. Amyloid-beta neuroprotection mediated by a targeted antioxidant. Sci Rep. 2014;4:4983.
51. Martinou JC, Youle RJ. Mitochondria in apoptosis: BCL-2 family members and mitochondrial dynamics. Dev Cell. 2011;21(1):92-101.
52. Brunelle JK, Letai A. Control of mitochondrial apoptosis by the BCL-2 family. J Cell Sci. 2009;122(Pt 4):437-41.
53. Perelman A, Wachtel C, Cohen M, Haupt S, Shapiro H, Tzur A. JC-1: alternative excitation wavelengths facilitate mitochondrial membrane potential cytometry. Cell Death Dis. 2012;3(11):e430-e.
54. Cenini G, Lloret A, Cascella R. Oxidative stress in neurodegenerative diseases: From a mitochondrial point of view. Oxid Med Cell Longev. 2019;2019:2105607.

55. Gay NH, Suwanjang W, Ruankham W, Songtawee N, Wongchitrat P, Prachayasittikul V, et al. Butein, isoliquiritigenin, and scopoletin attenuate neurodegeneration via antioxidant enzymes and SIRT1/ADAM10 signaling pathway. RSC Advances. 2020;10(28):16593-606.

56. Van Hau T, Ruankham W, Suwanjang W, Songtawee N, Wongchitrat P, Pingaew R, et al. Repurposing of nitroxolinedrug for the prevention of neurodegeneration. Chem Res Toxicol. 2019;32(11):2182-91.

57. Ruankham W, Suwanjang W, Wongchitrat P, Prachayasittikul V, Prachayasittikul S, Phopin K. Sesamin and sesamol attenuate H_2O_2-induced oxidative stress on human neuronal cells via the SIRT1-SIRT3-FOXO3a signaling pathway. Nutr Neurosci. 2019:1-12.

58. Gay NH, Phopin K, Suwanjang W, Songtawee N, Ruankham W, Wongchitrat P, et al. Neuroprotective effects of phenolic and carboxylic acids on oxidative stress-induced toxicity in human neuroblastoma SH-SY5Y cells. Neurochem Res. 2018;43(3):619-36.

59. Jin H, Kanthasamy A, Ghosh A, Anantharam V, Kalyanaraman B, Kanthasamy AG. Mitochondria-targeted antioxidants for treatment of Parkinson's disease: Preclinical and clinical outcomes. Biochim Biophys Acta. 2014;1842(8):1282-94.

60. Flynn JM, Melov S. SOD2 in mitochondrial dysfunction and neurodegeneration. Free Radic Biol Med. 2013;62:4-12.

61. Ren Z, He H, Zuo Z, Xu Z, Wei Z, Deng J. The role of different SIRT1-mediated signaling pathways in toxic injury. Cell Mol Biol Lett. 2019;24(1):36.

62. Xu J, Jackson CW, Khoury N, Escobar I, Perez-Pinzon MA. Brain SIRT1 mediates metabolic homeostasis and neuroprotection. Front Endocrinol 2018;9(702).

63. Salvatori I, Valle C, Ferri A, Carrì MT. SIRT3 and mitochondrial metabolism in neurodegenerative diseases. Neurochem Int 2017;109:184-92.

64. Shih J, Donmez G. Mitochondrial sirtuins as therapeutic targets for age-related disorders. Genes & Cancer. 2013;4(3-4):91-6.

65. Maiese K. Forkhead transcription factors: Formulating a FOXO target for cognitive loss. Curr Neurovasc Res. 2017;14(4):415-20.

66. Gomes BAQ, Silva JPB, Romeiro CFR, dos Santos SM, Rodrigues CA, Gonçalves PR, et al. Neuroprotective mechanisms of resveratrol in Alzheimer's disease: Role of SIRT1. Oxid Med Cell Longev. 2018;2018:8152373.

67. Gay N, Phopin K, Suwanjang W, Ruankham W, Wongchitrat P, Prachayasittikul S, et al. Attenuation of oxidative stress-induced neuronal cell death by *Hydnophytum formicarum* Jack. Asian Pac J Trop Med. 2018;11(7):415-22.

68. Jones MR, Mathieu E, Dyrager C, Faissner S, Vaillancourt Z, Korshavn KJ, et al. Multi-target-directed phenol–triazole ligands as therapeutic agents for Alzheimer's disease. Chem Sci. 2017;8(8):5636-43.

69. Montanari S, Mahmoud AM, Pruccoli L, Rabbito A, Naldi M, Petralla S, et al. Discovery of novel benzofuran-based compounds with neuroprotective and immunomodulatory properties for Alzheimer's disease treatment. Eur J Med Chem. 2019;178:243-58.

70. Adarsh N, Shanmugasundaram M, Ramaiah D. Efficient reaction based colorimetric probe for sensitive detection, quantification, and on-site analysis of nitriteions in natural water resources. Anal Chem. 2013;85(21):10008-12.

71. Guantai EM, Ncokazi K, Egan TJ, Gut J, Rosenthal PJ, Smith PJ, et al. Design, synthesis and *in vitro* antimalarial evaluation of triazole-linked chalcone and dienone hybrid compounds. Bioorg Med Chem. 2010;18(23):8243-56.

72. Efe C, Lykakis IN, Stratakis M. Gold nanoparticles supported on TiO_2 catalyse the cycloisomerisation/oxidative dimerisation of aryl propargyl ethers. ChemComm 2011;47(2):803-5.

73. Achard T, Lepronier A, Gimbert Y, Clavier H, Giordano L, Tenaglia A, et al. A regio- and diastereoselective platinum-catalyzed tandem [2+1]/[3+2] cycloaddition sequence. Angew Chem Int Ed. 2011;50(15):3552-6.

74. Lykakis IN, Efe C, Gryparis C, Stratakis M. Ph3PAuNTf2 as a superior catalyst for the selective synthesis of 2H-chromenes: Application to the concise synthesis of benzopyran natural products. Eur J Org Chem. 2011;2011(12):2334-8.

75. Hans RH, Guantai EM, Lategan C, Smith PJ, Wan B, Franzblau SG, et al. Synthesis, antimalarial and antitubercular activity of acetylenic chalcones. Bioorg Med Chem Lett. 2010;20(3):942-4.

76. Zammit SC, Cox AJ, Gow RM, Zhang Y, Gilbert RE, Krum H, et al. Evaluation and optimization of antifibrotic activity of cinnamoyl anthranilates. Bioorg Med Chem Lett. 2009;19(24):7003-6.

77. Tsuzuki Y, Nguyen TKN, Garud DR, Kuberan B, Koketsu M. 4-Deoxy-4-fluoro-xyloside derivatives as inhibitors of glycosaminoglycan biosynthesis. Bioorg Med Chem Lett. 2010;20(24):7269-73.

78. Hunt L, Jordan M, De Jesus M, Wurm FM. GFP-expressing mammalian cells for fast, sensitive, noninvasive cell growth assessment in a kinetic mode. Biotechnol Bioeng. 1999;65(2):201-5.

Table legend

Table1 Cell survival rate and cytotoxicity of chalcone-triazole derivatives[a,b]

Compound	% Viability		Cytotoxicity (IC_{50}, μg/mL)[d]
	Without H_2O_2	With H_2O_2	
Untreated	100.0 ± 0	63.94 ± 2.06*	-
6a	100.3 ± 1.09	87.82 ± 5.08#	> 50
6b	108.0 ± 6.51	57.66 ± 3.95	> 50
6c	96.86 ± 1.97	71.97 ± 2.12	> 50
6d	102.9 ± 4.05	75.87 ± 8.78	> 50
6e	98.36 ± 6.41	87.16 ± 1.99#	> 50
6f	91.09 ± 3.83	61.42 ± 1.12	> 50
6g	94.34 ± 4.90	65.02 ± 2.22	> 50
Resveratrol[c]	97.94 ± 0.25	86.08 ± 4.53#	ND[e]
Ellipticine[c]	ND[e]	ND[e]	0.724

[a] Significance: *$P < 0.05$ vs. the untreated cells; #$P < 0.05$ vs. the H_2O_2 group.

[b] The data are expressed as mean ± S.E.M.

[c] Resveratrol and ellipticine were used as the reference compounds.

[d] Cytotoxicity against Vero cells: IC_{50} > 50 μg/mL is defined as low cytotoxic effect.

[e] ND = not determined.

Figure legends

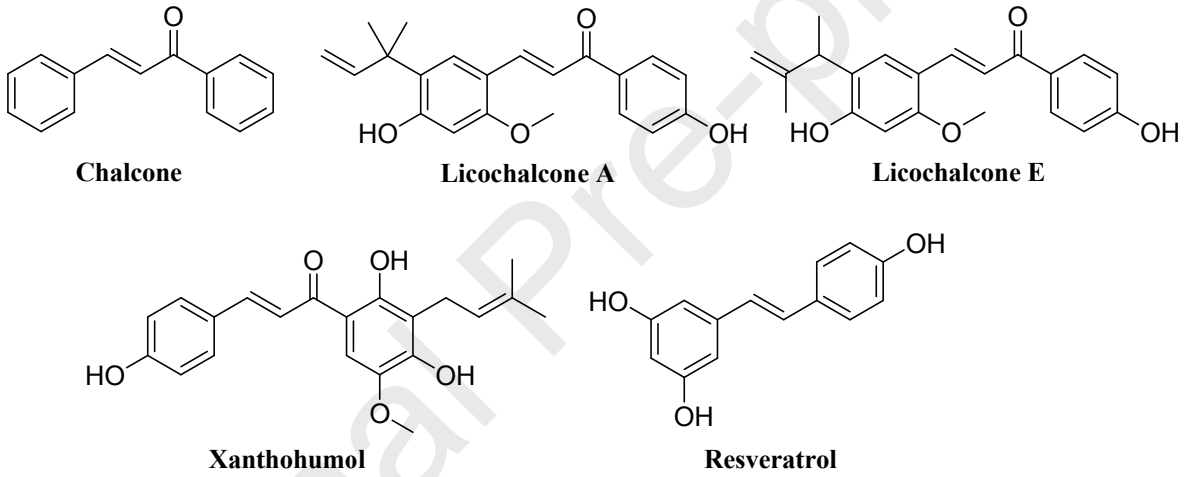

Fig. 1 Chemical structures of chalcone, licochalcones (A and E), xanthohumol and resveratrol

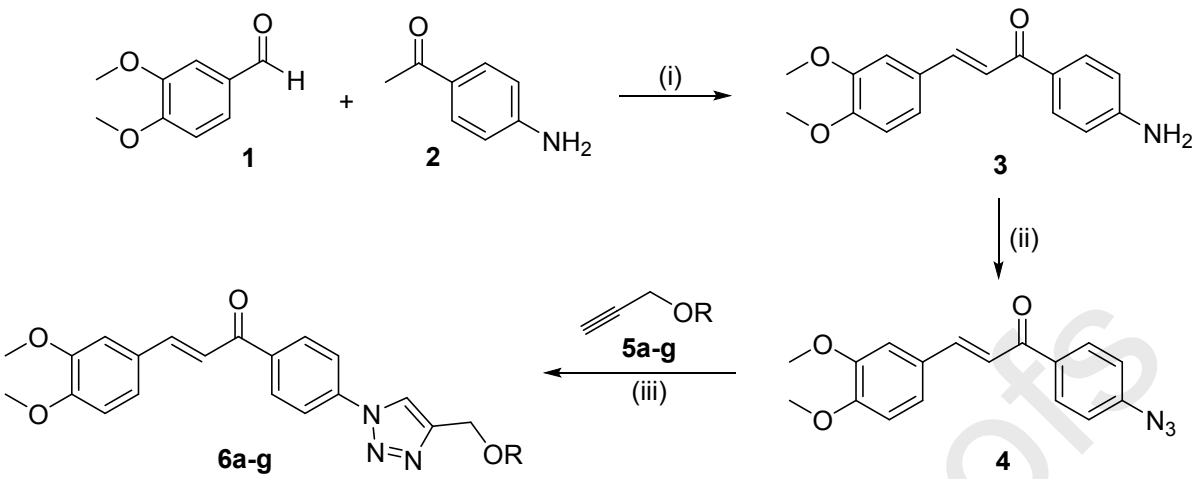

Reagents and conditions:
(i) 40% KOH, EtOH, rt
(ii) $NaNO_2$, HCl/CH_3COOH, 0 ^oC, 15 min then NaN_3, rt, 30 min
(iii) alkyne **5**, $CuSO_4 \cdot 5H_2O$, sodium ascorbate, *t*-BuOH/H_2O, rt

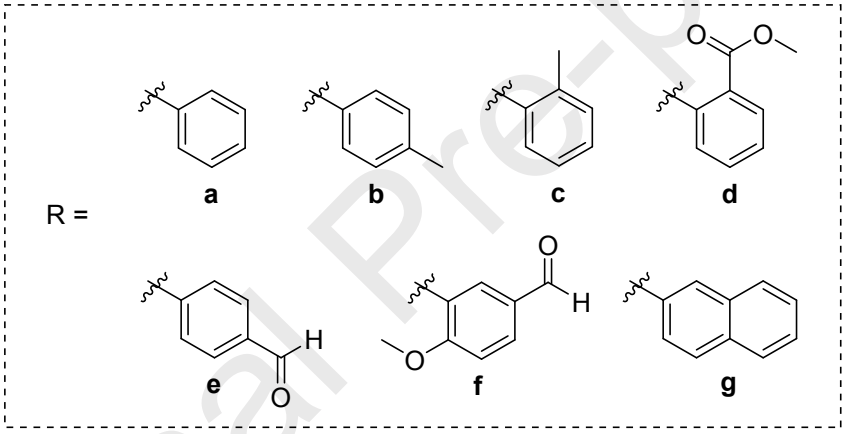

Scheme 1 synthesis of chalcone-triazole derivatives

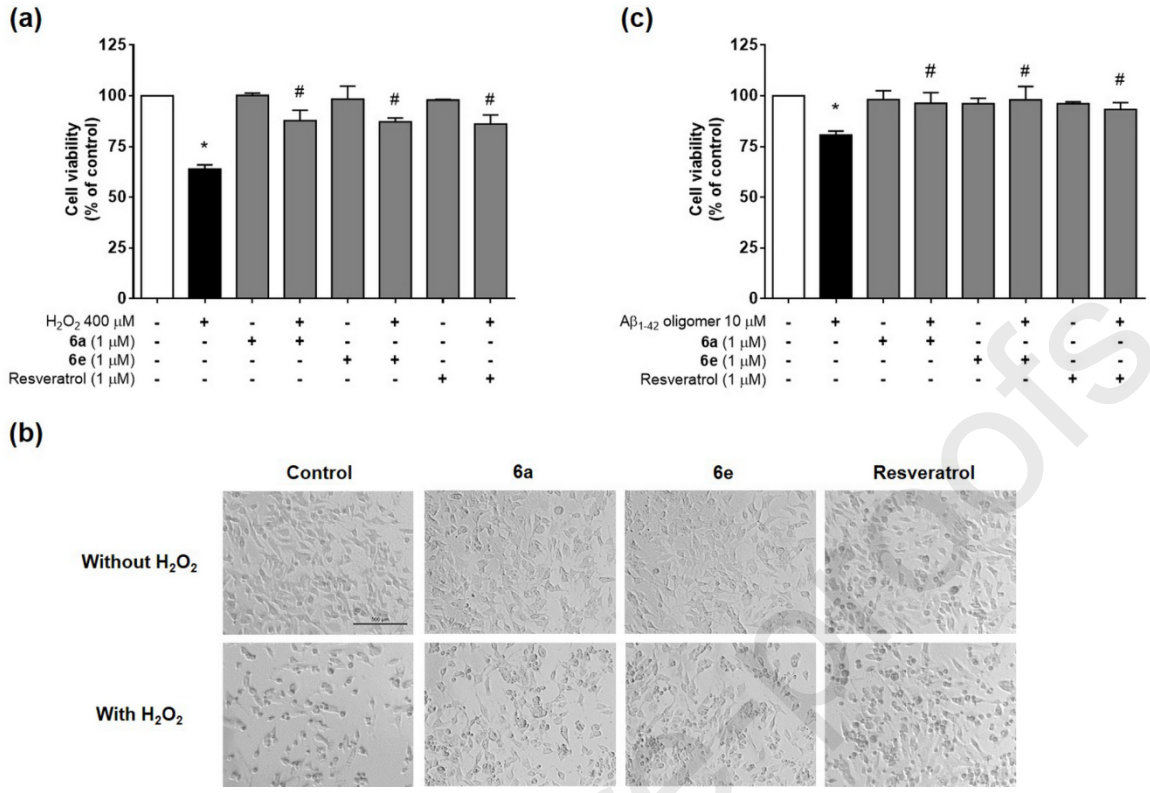

Fig. 2 Chalcone-triazole derivatives (**6a** and **6e**) alleviate the cytotoxic effect in the neuronal cells. (a) The SH-SY5Y cells were incubated with 1 μM of **6a**, **6e**, or resveratrol for 3 h followed by 400 μM H_2O_2 for 24 h, and evaluated by MTT assay. (b) Morphological alteration was observed under a light microscope (20X magnification). Scale bar = 200 μm. (c) The cells were preincubated with compounds followed by 10 μM $A\beta_{1\text{-}42}$ oligomer for 3 h, and evaluated by MTT assay. The data are expressed as mean ± S.E.M. $^{*}P < 0.05$ compared with the control cells; $^{\#}P < 0.05$ compared with the H_2O_2 or $A\beta_{1\text{-}42}$ oligomer groups.

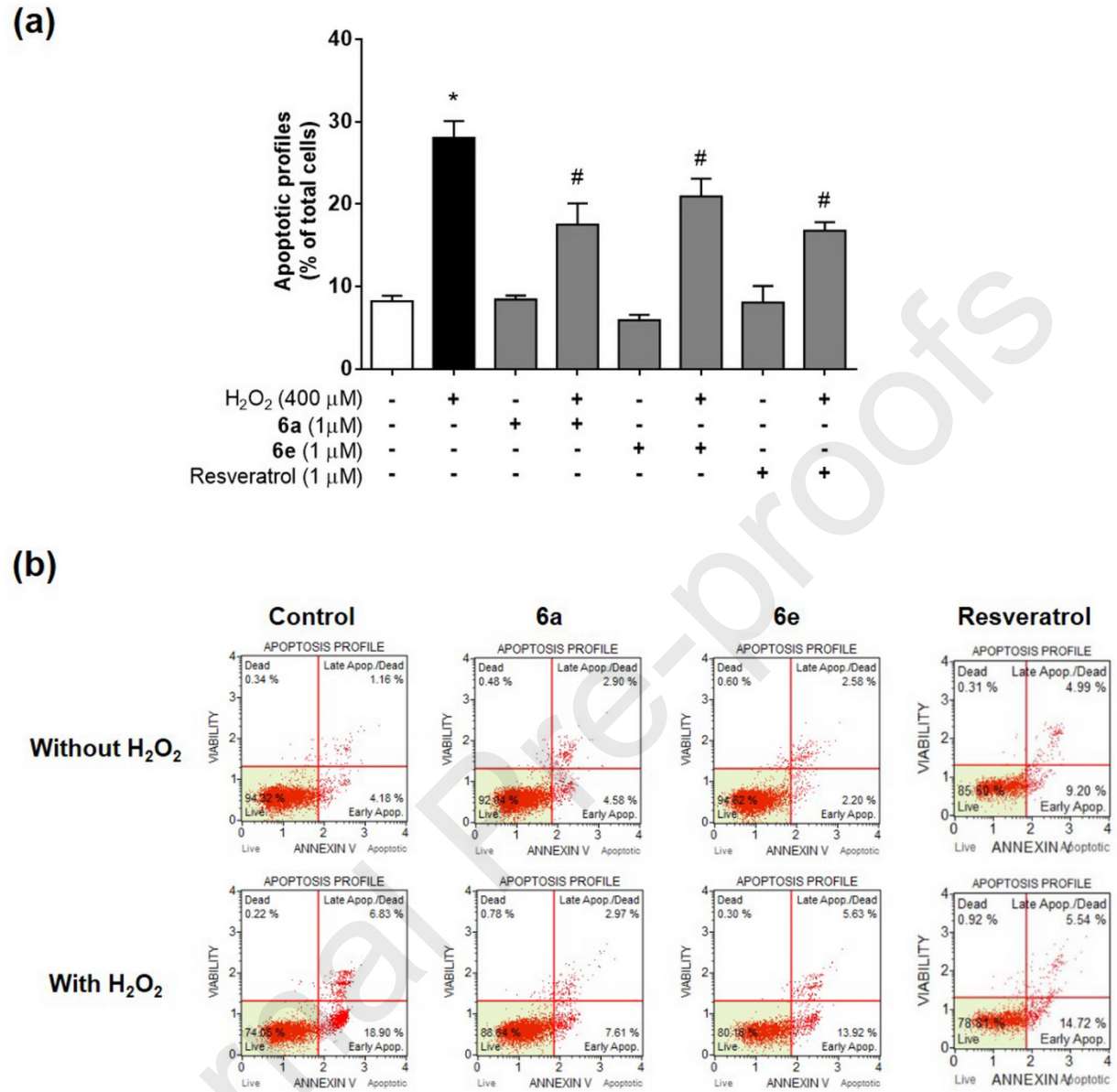

Fig. 3 Chalcone-triazole derivatives (**6a** and **6e**) inhibit H_2O_2-induced apoptosis in SH-SY5Y cells. (a) Apoptotic profiles were determined by annexin V/7-AAD. (b) Flow cytometric plots represented the percentages of live, early apoptotic, late apoptotic, or necrotic cells. The data are expressed as mean ± S.E.M. $^{*}P < 0.05$ compared with the control; $^{\#}P < 0.05$ compared with the H_2O_2 group.

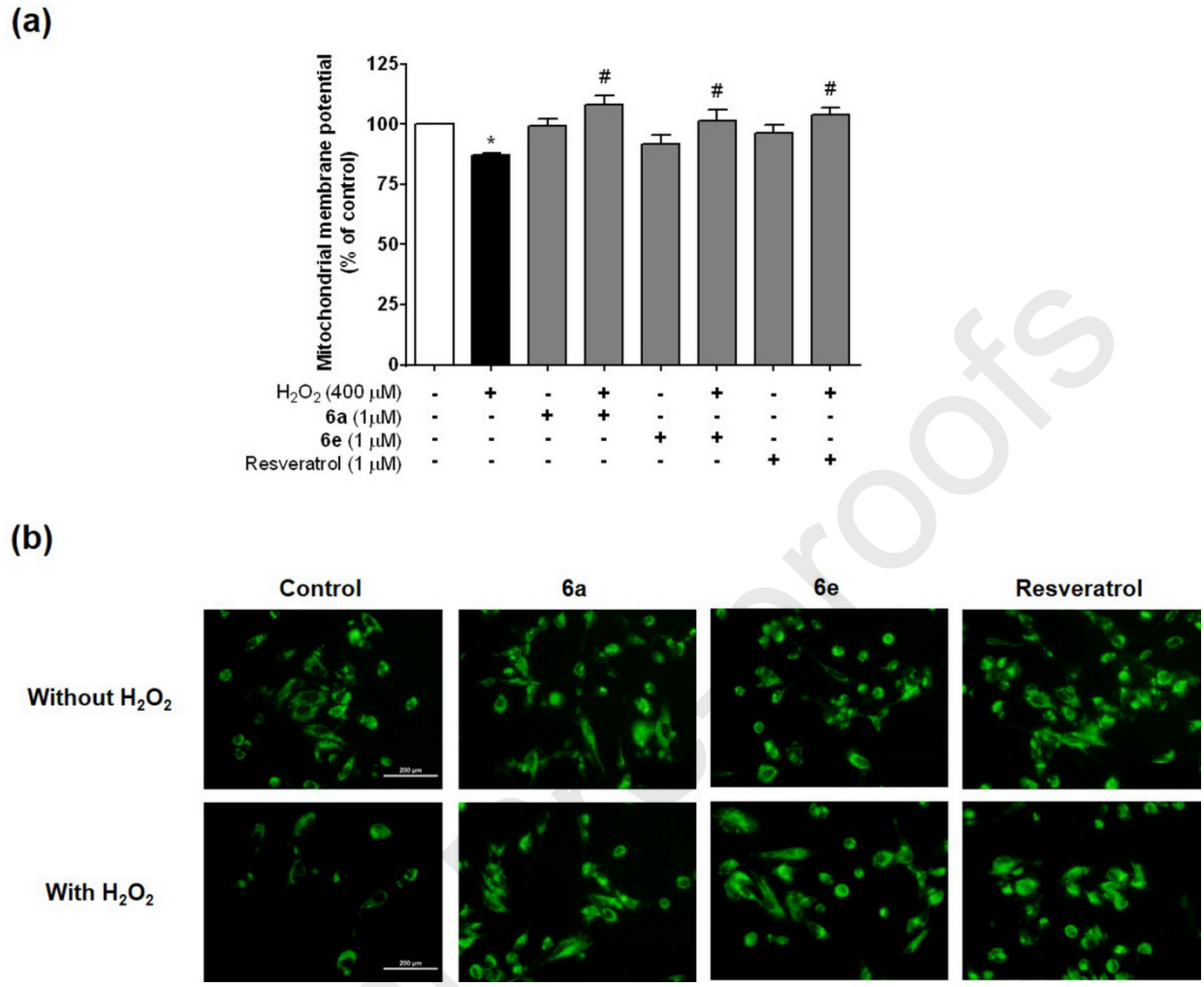

Fig. 4 Chalcone-triazole derivatives (**6a** and **6e**) maintain mitochondrial membrane potential of SH-SY5Y cells against oxidative stress. Mitochondrial membrane potential was measured by (a) fluorescence spectrophotometer and photographed by (b) fluorescence microscopy (20X magnification). Scale bar = 200 μm. The data are expressed as mean ± S.E.M. $^{*}P < 0.05$ compared with the untreated cells; $^{\#}P < 0.05$ compared with the H_2O_2 group.

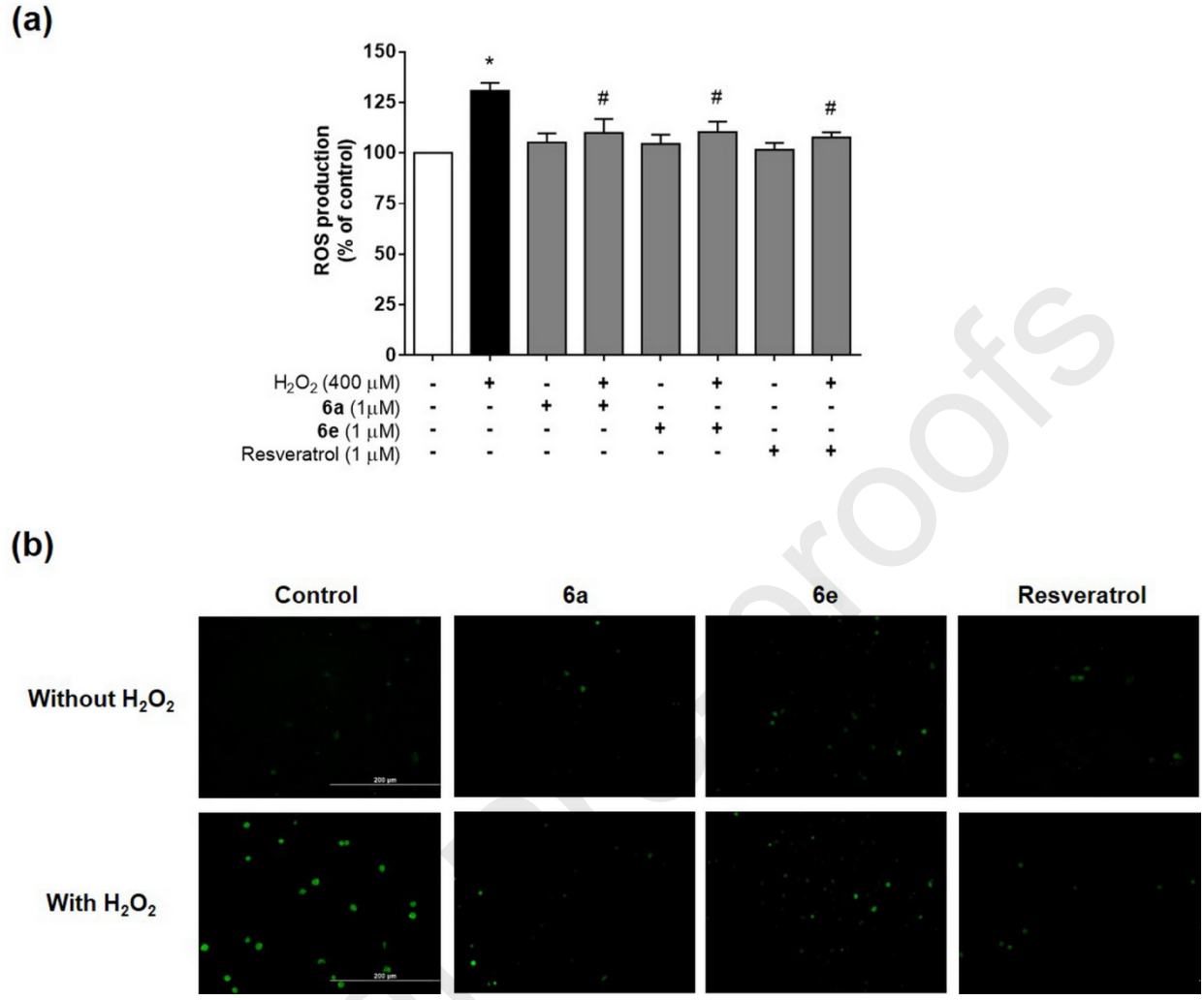

Fig. 5 Chalcone-triazole derivatives (**6a** and **6e**) reduce H_2O_2-induced ROS production in SH-SY5Y cells. (a) Measurement of ROS levels was determined by carboxy-DCFDA assay. (b) Representative fluorescence microscopy images were observed by a fluorescence microscope (20X magnification). Scale bar = 200 μm. The data are expressed as mean ± S.E.M. $^{*}P < 0.05$ compared with the control; $^{\#}P < 0.05$ compared with the H_2O_2 group.

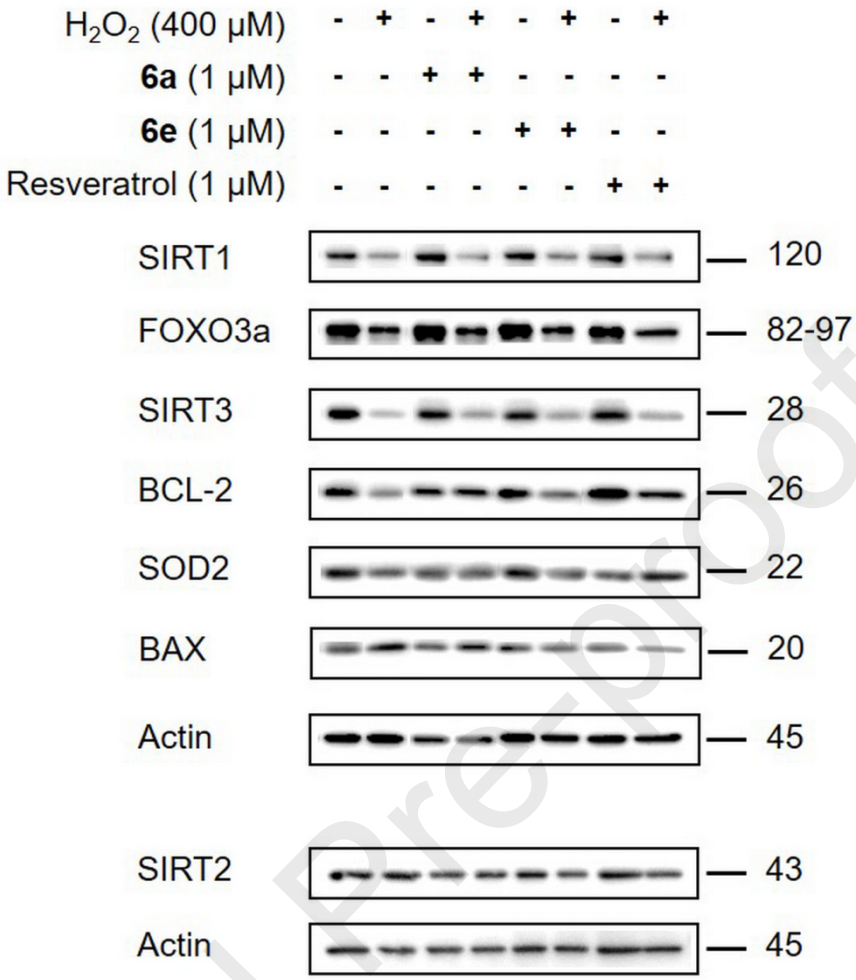

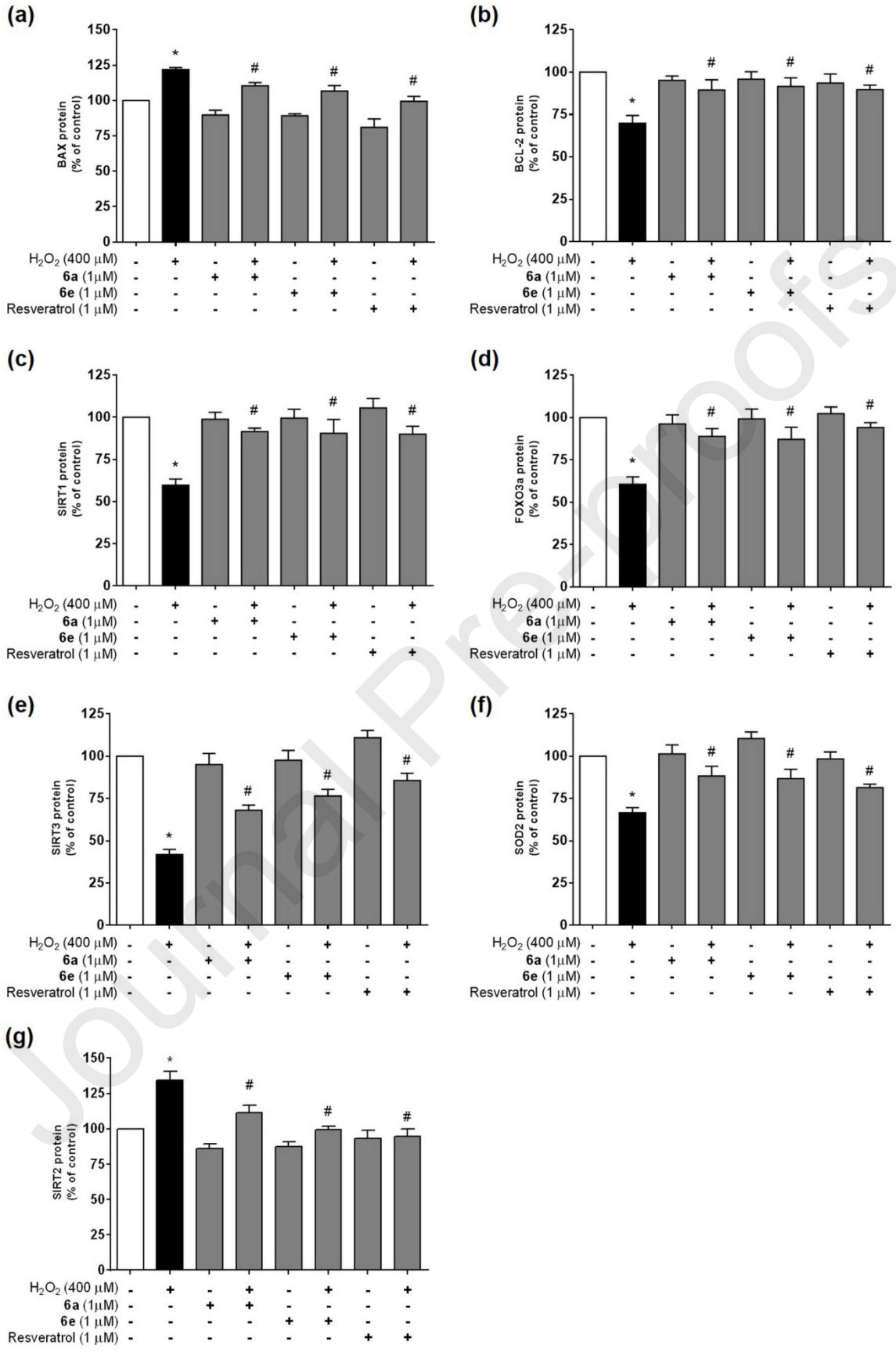

Fig. 6 Chalcone-triazole derivatives (**6a** and **6e**) inhibition of H_2O_2-induced oxidative damage is mediated by SIRT1/2/3-FOXO3a signal pathway in SH-SY5Y cells. Modulation of **6a** and **6e** on the protein levels of (a) BAX, (b) BCL-2, (c) SIRT1, (d) FOXO3a, (e) SIRT3, (f) SOD2, and (g) SIRT2 were determined by Western blot analysis. The data are expressed as mean ± S.E.M. $^{*}P < 0.05$ compared with the untreated cells; $^{\#}P < 0.05$ compared with the H_2O_2 group.

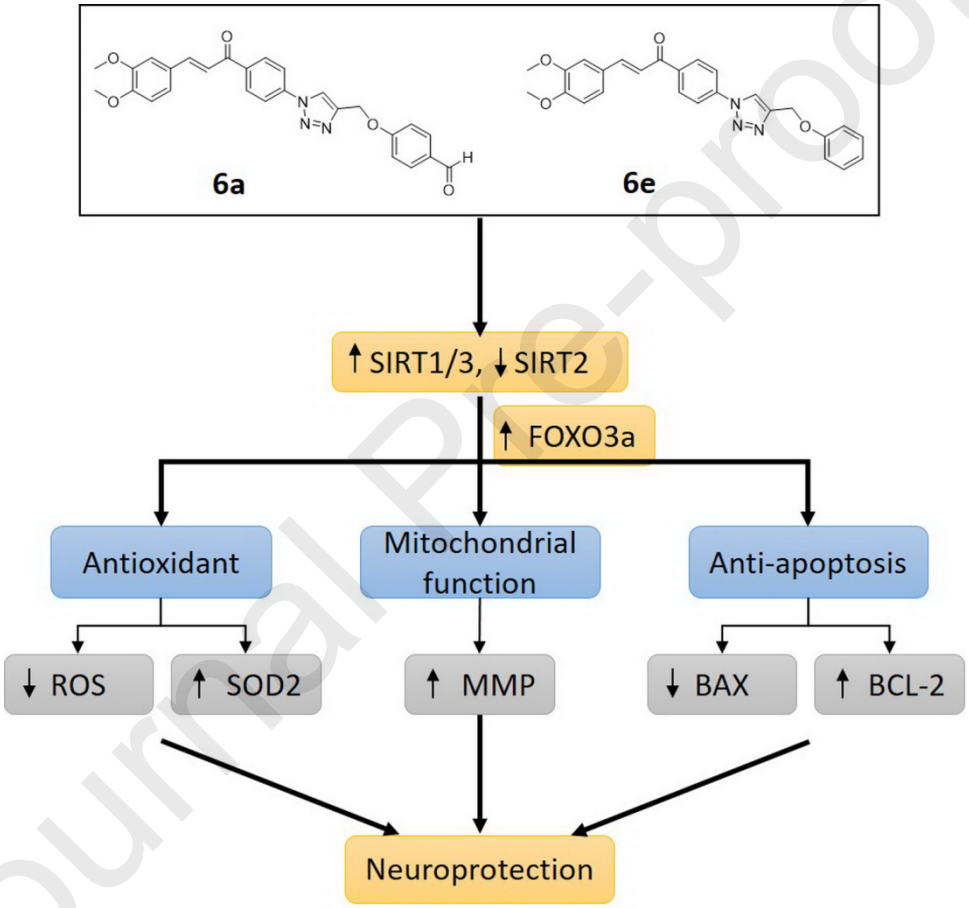

Fig. 7 The possible mechanisms of chalcone-triazole derivatives (**6a** and **6e**) against H_2O_2-induced oxidative stress through SIRT1/2/3-FOXO3a pathway.

Graphical abstract

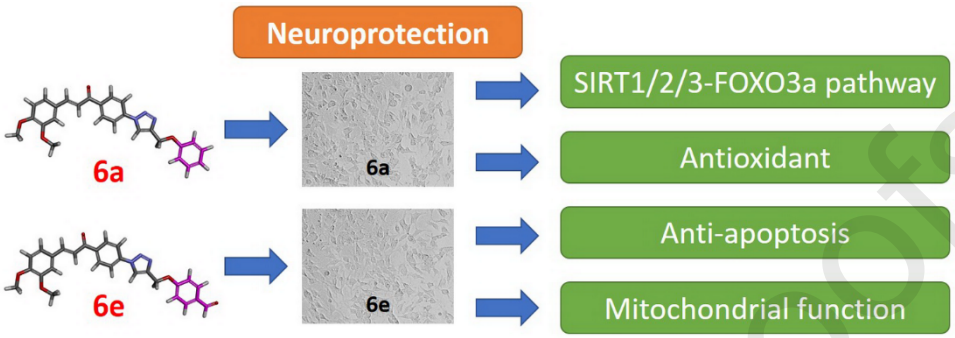

► Novel chalcone-triazole hybrids were synthesized.

► Chalcone-triazole derivatives protect neuronal cell death and maintain cellular antioxidant status without cytotoxicity.

► Cell Morphology and cell survival rate of neurons-treated by H_2O_2 were clearly improved by chalcone-triazole compounds.

► SIRT1/2/3-FOXO3a signaling pathway involves in neuroprotective effects of chalcone-triazole derivatives.

The authors declare no competing financial interest.